Hindawi
International Journal of Antennas and Propagation
Volume 2022, Article ID 5281470, 10 pages
https://doi.org/10.1155/2022/5281470

Research Article

Wideband Low-Profile 8 × 8 MIMO Antenna Based IFA Pair for Ultrathin 5G Smartphones

Hui Zhou, Di Wu, Mingmin Zhu, Yang Qiu, Guoliang Yu, and Hao-Miao Zhou

Key Laboratory of Electromagnetic Wave Information Technology and Metrology of Zhejiang Province, College of Information Engineering, China Jiliang University, Hangzhou 310018, China

Correspondence should be addressed to Hao-Miao Zhou; zhouhm@cjlu.edu.cn

Received 3 February 2022; Revised 16 April 2022; Accepted 21 April 2022; Published 14 May 2022

Academic Editor: Mohammad Alibakhshikenari

In this paper, a wideband 8 × 8 MIMO antenna is proposed. The proposed antenna can realize the low profile of 4 mm and the 3.18–4.40 GHz broadband coverage only by adjusting the ground edge structure of the deformed inverted-F antenna. Based on the original antenna, the 5G new radio (NR) band n77 (3.3–4.2 GHz) can be covered without adding any structure. In addition, the coupling between the antenna elements has also been improved, decreasing from −9.7 dB to −13.37 dB. A dual-element IFA pair is simulated, fabricated, and measured, the results show the bandwidth of 3.07–4.43 GHz, and the isolation of −13.89 dB can be achieved. An eight-element MIMO antenna is formed by placing four sets of antenna pairs along the two long edges of the substrate. The experimental results show that the bandwidth is 3.18–4.40 GHz, the isolation between any two ports is better than −12.25 dB, and the total efficiency is 61.14%–93.97%. By placing the planar antenna vertically, the ground clearance of the antenna can be reduced to zero, and the performances are similar to the planar MIMO antenna. The proposed MIMO antenna has a good profile and efficient radiation performance compared with the other works, so it has an important application value in ultrathin 5G smartphones.

1. Introduction

In recent years, with the rapid development of mobile communication, higher requirements have been put forward for the channel capacity and data transmission rate. The key technology of multiple-input multiple-output (MIMO) can significantly improve channel capacity and spectrum efficiency [1], so it has attracted wide attention. According to the division of 3GPP, the fifth-generation new radio (5G NR) communication system includes two frequency ranges: 450–6000 MHz (sub-6 GHz) and 24250–52600 MHz (millimeter wave) [2]. At present, the frequency bands most likely to be preferentially deployed in the world are 3.3–4.2 GHz (n77, n78) and 4.4–5.0 GHz (n79) [3–5]. As the most common carrier in the mobile communication system, smartphones need to apply MIMO antenna systems to achieve fast data transmission. By integrating multiple antenna elements into the smartphone, the spectrum resources can be utilized efficiently, and the channel capacity can be increased. However, nowadays, the smartphone is getting thinner and thinner, while it integrates increasingly smart devices, leaving less and less space for the mobile phone antenna. Using multiple single-band antennas to cover the 5G NR band will increase the number of antennas and occupy more space resources. Therefore, the design of a wideband low-profile MIMO antenna has become the current research hotspot [6].

The existing 5G mobile phones usually need 4–8 antenna elements of the same frequency to send and receive signals together. Due to the close distance between the elements, there is near-field coupling, which leads to decreased antenna data transmission efficiency. Therefore, it is essential to maintain low coupling and low envelope correlation coefficient (ECC) between antenna elements [7]. To eliminate the interference caused by the near-field coupling between MIMO antenna elements, the most direct decoupling method is to place separately [8–11]. In [11], eight bent monopole antennas in the 5G band are arranged along the

long side, and a rectangular area is excavated from the ground plane below the antenna as the clearance area of the antenna. Finally, the antenna array can achieve −10 dB isolation across the 3.4–3.6 GHz band. Clearly, separate placement will be limited by smartphone space. To this end, many studies have proposed highly integrated antenna structures [12–17] and reduced the coupling through additional decoupling methods, such as adding neutralization lines [18]and lumped elements [19, 20], or designing defective grounds [21] and pattern diversity structures [22]. Sun et al. [12] proposed a compact antenna pair that uses the structural characteristics of the antenna itself, the orthogonal mode of current direction excited by different ports can realize the low coupling effect when the antennas are closely arranged. In [19], the adjacent antenna elements are tightly arranged at a distance of 1 mm. The isolation is lower than −11.6 dB by adding capacitors and inductors. In [22], pattern diversity is achieved by using in-phase and out-of-phase signals, and its isolation is lower than −14 dB. In addition, shared radiator antennas have been proposed by researchers [23, 24]. Chen et al. [24] designed the shared radiation patch, which is connected by two grounding strips and two feed ports. By adjusting the distance of the feed port and the position and size of the grounding strip, a high isolation characteristic of –20 dB can be achieved. However, most of these antennas are narrowband antennas operating at 3.4–3.6 GHz, which cannot cover most of the 5G NR application bands.

In recent years, wideband antennas covering n77, n78, n79, or even wider bands have become a new trend in 5G antenna designs. Compared with the narrowband decoupling of single-band antennas, it is more challenging to maintain low coupling between elements over the wideband [25, 26]. For example, Y. Hei et al. [25] proposed a wideband MIMO antenna, both parasitic strip and defective ground structure are used to achieve high isolation characteristics of –15 dB. In [27], a dual-band antenna covering 3.3–4.2 GHz and 4.8–5 GHz was designed, and a T-stub is placed between the elements to achieve an isolation lower than −12.5 dB. However, the size of the decoupling structure is too large, resulting in low antenna integration. Two self-decoupled wideband antennas covering 3.3–5 GHz are proposed in [28, 29], which isolations are −12.0 dB and −10 dB, respectively. These two antenna elements are tightly arranged and small, but the efficiency of some antenna elements is only about 40% over the bandwidth range. Reference [30] proposed a self-decoupled antenna with an overall efficiency greater than 73% and a bandwidth of 3.3–4.2 GHz, but the size is large, and there is still a lot of room for improvement. Surely, the design of multielement 5G smartphone antennas with miniaturization, wideband, low coupling, and high efficiency is still facing great challenges.

In this paper, a low-profile miniaturized 5G wideband 8×8 MIMO antenna with an element size of 18.6 mm × 4 mm and a distance of only 0.8 mm between adjacent elements is presented. To reduce the profile height of the inverted-F antenna, the antenna structure is optimized. By adjusting the ground structure under the element feed port, the bandwidth of the antenna pair is widened from 230 MHz to 1440 MHz (3.06–4.50 GHz), so that the 5G n77 and n78 frequency bands can be completely covered. The adjusted ground structure suppresses the coupling current of the antenna pair and reduces the isolation from −9.7 dB to −13.37 dB. On the basis of the proposed low coupling antenna pair, an 8-element mobile phone antenna is designed. Compared with the existing 5G wideband MIMO mobile phone antenna, the profile height of the proposed 8×8 MIMO antenna is only 4 mm, and the efficiency is as high as 93.97%. The measured coupling between the elements is lower than −12.25 dB. It has obvious advantages in bandwidth, antenna size, isolation, and efficiency.

2. Evolution and Design of Wideband Antenna Pair

The evolution of the wideband antenna pairs is shown in Figure 1. Both the antenna pair and the ground are printed on the substrate of 150 mm × 75 mm × 0.8 mm, and the substrate material is FR-4($\varepsilon r = 4.4$, $\tan\delta = 0.02$). Due to the simple structure of the inverted-F antenna, the impedance matching is easier to adjust. When the inverted-F antenna resonates, the current is mainly distributed in the horizontal open-circuit branch and short-circuit branch, while there is basically no current distribution in the feeding branch. Therefore, the inverted-F antenna shall be properly deformed to make the feeding branches of the two adjacent antenna elements and reduce the coupling of the two adjacent antenna elements as much as possible. The deformed antenna element is shown in Case 1 in Figure 1(a), the distance between the two antenna elements is 0.8 mm, and the profile height of the antenna is 4 mm. The S and Z parameters are simulated and analyzed by high-frequency electromagnetic field simulation software, and the results are shown in Figures 2(a) and 2(b). It can be observed that the antenna bandwidth of Case 1 is only 240 MHz, and the isolation is less than −9.7 dB. To broaden the bandwidth of the antenna, the edge structure of the ground in Case 1 is adjusted and designed to obtain Case 2 as shown in Figure 1(b). The antenna element of Case 2 reduces the contact area between the grounding branch and the ground and prolongs the current path of the antenna. Therefore, the self-impedance of the antenna is improved, which is close to 50 Ω in the frequency band range of 3.47–4.23 GHz, and the −6 dB bandwidth can realize 760 MHz. However, the coupling of antenna pairs has not been improved. To reduce the coupling of antenna pairs, the edge structure connected to the ground under the two antenna elements in Case 2 is further improved, and the Case 3 structure shown in Figure 1(c) is obtained. Case 3 reduces the contact area between the feeding branches and the ground and blocks the coupling current between the antenna elements. It can be observed from Figure 2(a) that the S21 of the antenna in Case 3 decreases from −9.7 dB to −13.37 dB, and the isolation is greatly improved. When fed through port 1, the surface current distribution of the antenna pair in Case 1 and Case 3 is shown in Figures 2(c) and 2(d). Due to the adjustment of the edge structure of the ground under the antenna element feeding branch, the current intensity flowing from the

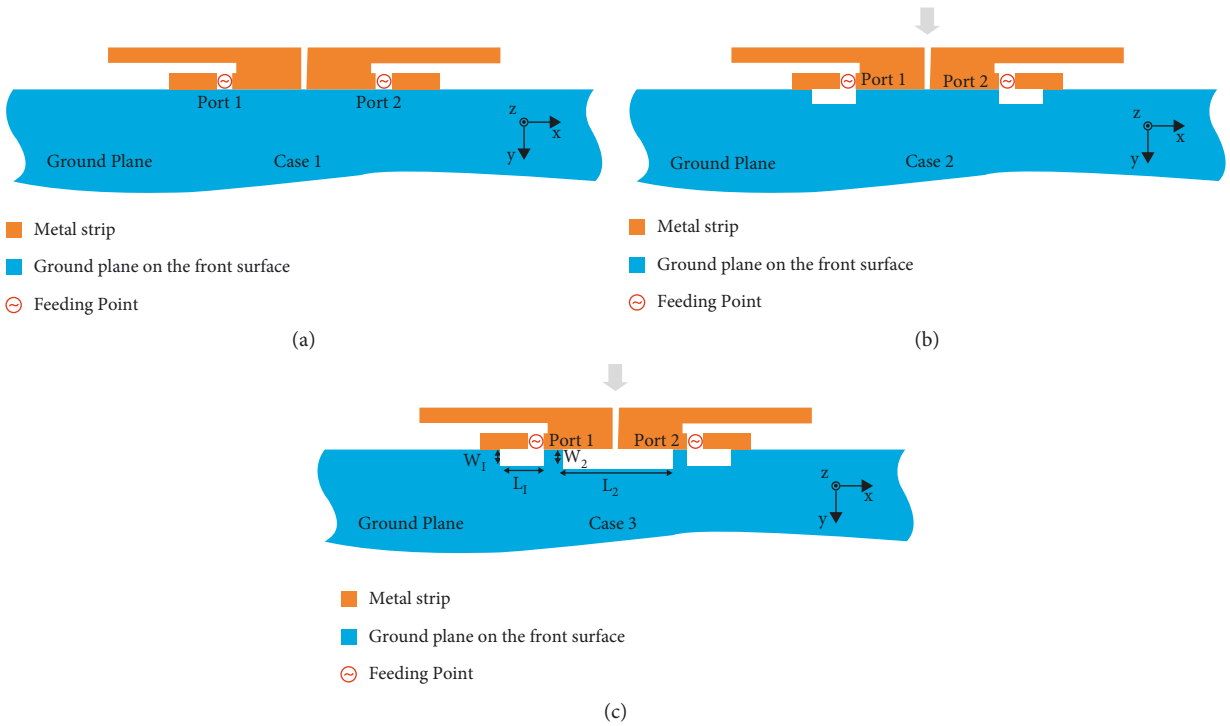

Figure 1: Evolution procedure of the proposed antenna pair.

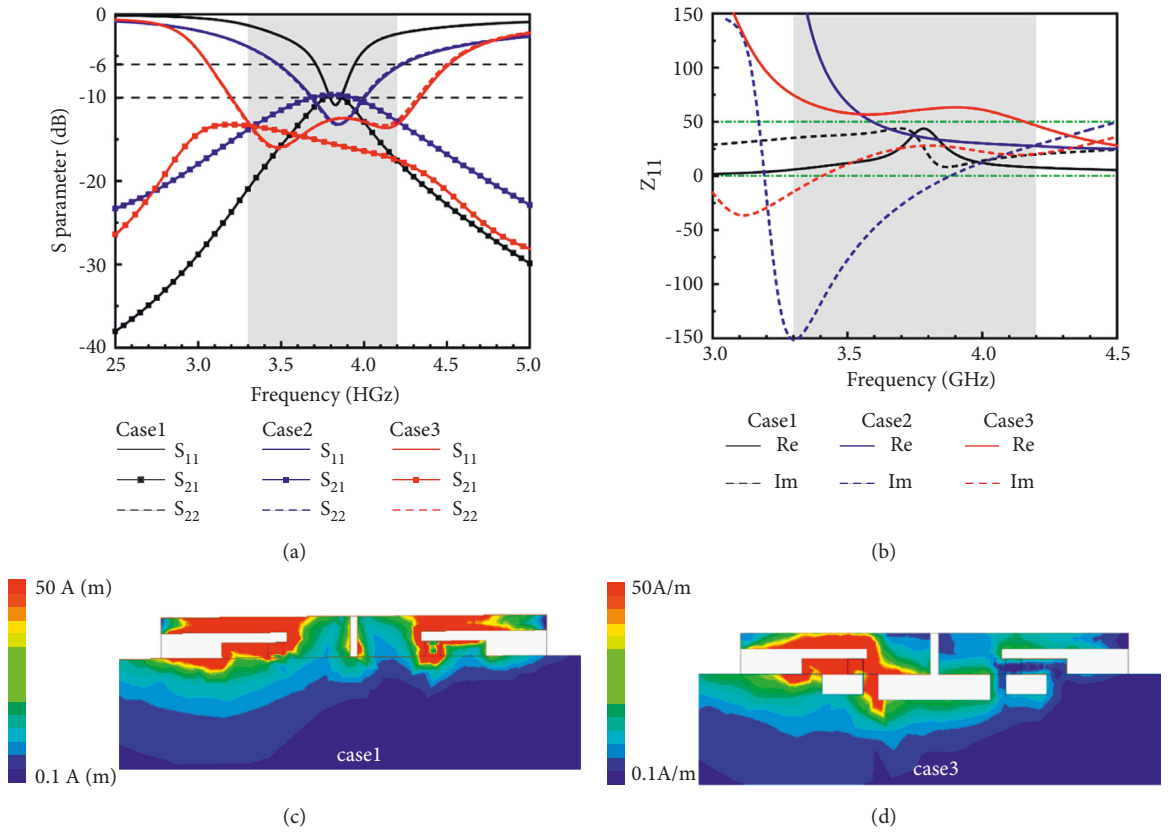

Figure 2: Comparison of the antenna pairs proposed in Case 1–Case 3. (a) S parameter. (b) Z11. (c), (d) Simulated surface current distributions of the antenna pair in Case 1 and Case 3.

ground into the adjacent antenna elements is greatly weakened, which makes the current intensity of the antenna element where port 2 is located in Case 3 very weak and improves the isolation of the antenna within the target frequency band. In addition, the adjusted ground edge can also be used as a radiation slot to broaden the working bandwidth of the antenna. The impedance matching of the antenna is improved in the range of 3.06–4.50 GHz, and the bandwidth reaches 1440 MHz.

From the above analysis, it can be seen that the edge structure of the ground has a great influence on the performance of the antenna. Therefore, the parameters L1, W1, L2, and W2 of the ground edge structure in Case 3 are analyzed, and the results are shown in Figure 3. Among them, L1 and W1 affect the contact area between the grounding branch and the ground plane. When the values of L1 are 2.5 mm, 4 mm, and 5.5 mm, respectively, as shown in Figure 3(a), the resonant frequency shifts to high frequency, and the coupling is decreased clearly. It can be seen that the value of W1 has little effect on the bandwidth and isolation from Figure 3(b), but the resonance depth will become deeper with the increase of W1. L2 and W2 affect the contact area between the feeding branch and the ground plane. When the values of L2 are 12 mm, 11 mm, and 10 mm, respectively, as shown in Figure 3(c), the coupling decreases with the decrease of L2, and the resonance depth becomes deeper, but the bandwidth decreases slightly. Similarly, it can be seen that the resonance depth will be significantly shallower with the increase of W2 from Figure 3(d), the bandwidth will be slightly larger, and the isolation will not change significantly. Through the above analysis, the above four parameters are optimized and selected as $L1 = 4\,\text{mm}$, $W1 = 2\,\text{mm}$, $L2 = 11\,\text{mm}$, $W2 = 2.5\,\text{mm}$.

The geometry and size of the optimized MIMO antenna pair are shown in Figure 4(a). The size of the antenna element is $18.6\,\text{mm} \times 4\,\text{mm}$, and the distance from edge to edge of adjacent antenna elements is only 0.8 mm. The antenna pair is placed at the center of the long side of the substrate and printed on the upper surface of the substrate together with the metal ground ($150\,\text{mm} \times 75\,\text{mm}$). The far-field radiation pattern of the antenna pair is analyzed by using high-frequency simulation software. When port 1 of the antenna pair is excited, the antenna radiates strongly on the left and hardly on the right, as shown in Figure 4(b). Similarly, when feeding through port 2, the antenna radiation is mainly concentrated on the right, while the left hardly radiates, as shown in Figure 4(c). The maximum radiation direction of Ant1 mainly points to the x-direction, while that of Ant2 directs to the -x direction. Using this radiation characteristic, the antenna pair can obtain good radiation pattern diversity performance, greatly reducing the coupling between the two antenna elements, and thus resulting in low ECCs.

To verify the performance of the designed antenna pair, the antenna is fabricated, and the S parameters are measured by the Agilent N5230C vector network analyzer. The results are shown in Figure 5(a). All ports are fed with a $50\,\Omega$ semiflexible coaxial line. The simulated −6 dB bandwidth for port 1 and port 2 is 1440 MHz (3.06–4.50 GHz), and the measured result is 1360 MHz (3.07–4.43 GHz). In the n77 frequency band, the simulated S21 is lower than −13.37 dB, and the measured S21 is lower than −13.89 dB. The simulated and measured bandwidth and isolation are consistent, and the measured isolation is even better than the simulation result. During antenna processing, there may be defects in the welding between the coaxial line and the feed port, which changes the impedance matching of the connection, resulting in a slight difference between the measured return loss results and the simulation results. The efficiency of the proposed antenna is measured in a dark room, and the results are shown in Figure 5(b). The efficiency of the antenna fed by port 1 is 71.11%–92.14%, while that fed by port 2 is 68.04%–86.79%, slightly lower than that of port 1. The average efficiency over the entire operating frequency band is 77.22%.

3. Design of the 8×8 MIMO Antenna

Using the wideband antenna pair designed in the previous section, an 8×8 MIMO antenna is further designed. The distribution and size of the 8-element antenna on the substrate are shown in Figure 6(a). By placing four sets of wideband antenna pairs of the same size as Figure 4(a) on the long side of the FR-4 substrate, an 8×8 MIMO antenna system can be realized. Antenna pairs on the same long side have a distance of 36 mm between each other. To suppress the mutual interference between antenna pairs, a rectangular slot of $18\,\text{mm} \times 0.5\,\text{mm}$ is etched at the center of the long side of the ground to block the coupling current between adjacent antenna elements of different antenna pairs (port 2 and port 3, port 6 and port 7). The fabricated 8×8 MIMO antenna is shown in Figure 6(b).

The simulated and measured reflection coefficients of the eight-element antenna are shown in Figure 7. Considering the symmetry of the structure, only the reflection coefficients of port 1, port 2, port 3, and port 4 are given. The simulated −6 dB bandwidth of port 1 and port 4 is 1460 MHz (3.07–4.53 GHz), and the simulated −6 dB bandwidth of port 2 and port 3 is 1370 MHz (3.16–4.53 GHz). The measured −6 dB bandwidth of port 1 and port 4 is 1320 MHz (3.15–4.47 GHz), and the measured -6 dB bandwidth of port 2 and port 3 is 1220 MHz (3.18–4.40 GHz). The overlapping −6 dB bandwidth is 1220 MHz (3.18–4.40 GHz), which is sufficient to fully cover the 3.3–4.2 GHz band. Due to the manual manufacturing error and influence of the test coaxial line, there is little difference between the simulation and measured results. In the expected n77 frequency band, the impedance matching between the simulation results and the measured results is better than −6 dB.

The isolation between different antenna pairs is measured experimentally, and the results are shown in Figure 8. Figure 8(a) shows the mutual coupling between the two antenna pairs with the same long side. It can be seen that in the n77 frequency band, the isolation between port 1 and port 2 is −14.95 dB, and the isolation between port 2 and port 3 is −12.25 dB. The isolation between any two ports on the same long side is less than −12.25 dB. Figure 8(b) shows the mutual coupling between ports with different long sides. It can be seen that the isolation between any two ports is lower than −22.42 dB.

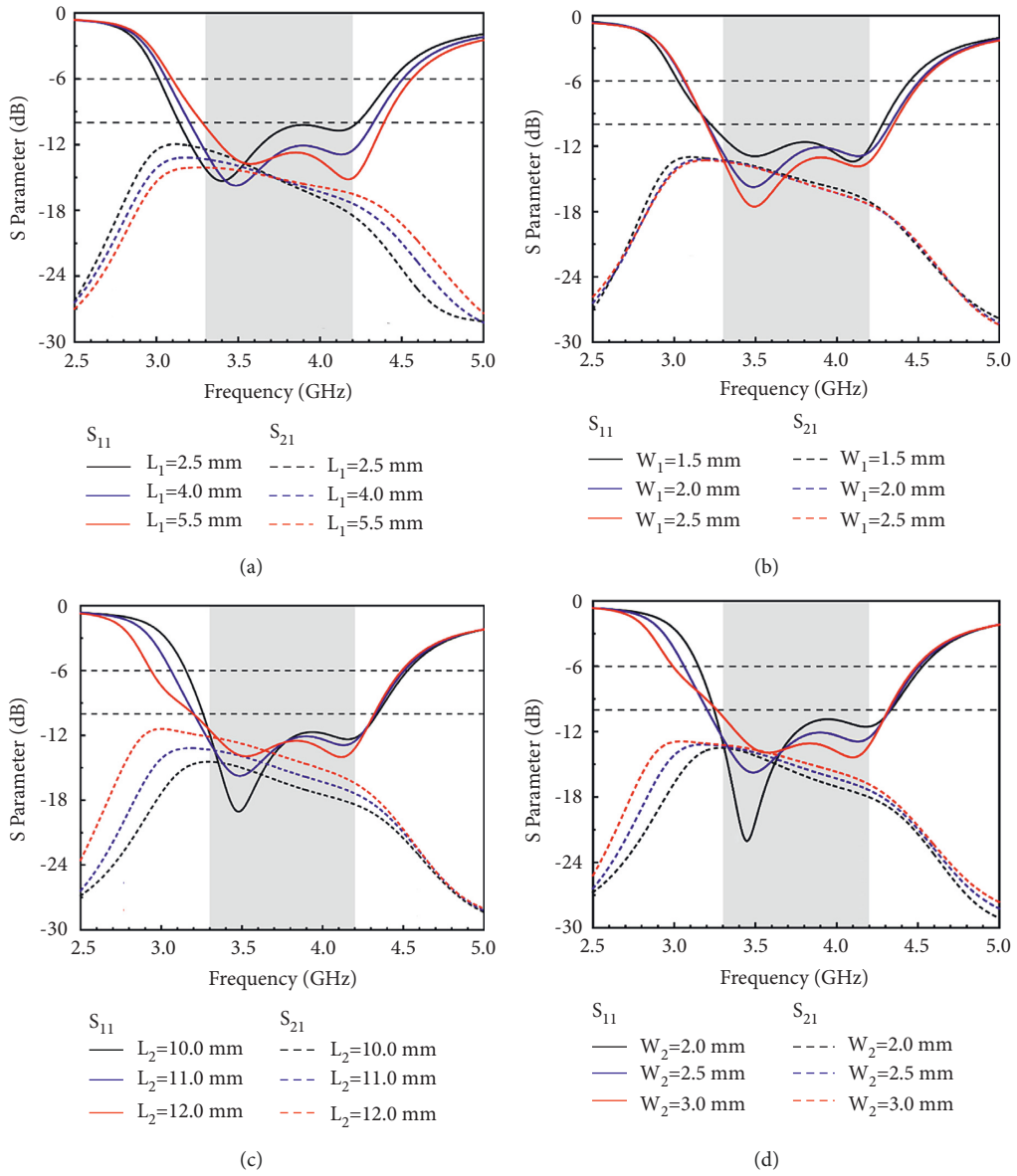

Figure 3: Simulated S parameter with different values of (a) L1, (b) W1, (c) L2, and (d) W2.

In addition, the radiation performance of the antenna is measured in the microwave anechoic chamber. During the measurement, when one port is connected to the test line, the remaining seven ports are terminated with 50 Ω loads. The efficiency and calculated ECC according to the radiation patterns are shown in Figure 9(a), and the gains are shown in Figure 9(b). In the n77 frequency band, when port 1 is fed, the efficiency of the antenna is 71.91%–93.97%, the average efficiency is 84.54%, and the realized peak gain is 2.81–7.97 dBi. The efficiency of the antenna fed by port 2 is 61.14%–85.34%, the average efficiency is 74.07%, and the realized peak gain is 3.15–6.61 dBi. In addition, the efficiency of port 1 is higher than that of port 2, because the slot etched between two antenna pairs affects the efficiency of antenna 2. In the 3.3–4.2 GHz band, the ECC between port 1 and port 2 is lower than 0.16, the ECC between port 2 and port 3 is lower than 0.17, and the ECC between port 2 and port 3 can be as low as 0.08. In conclusion, the ECC between all ports of the proposed 8-element antenna is lower than 0.17 in the range of 3.3–4.2 GHz, which meets the standard requirements for 5G smartphones.

In the above 8 × 8 MIMO antenna design, the profile of the antenna pair is 4 mm, which means that the ground clearance between the frame and the ground is at least 4 mm, so it may not be suitable for some narrow frame smartphones. To this end, some improvements are made to the wideband antenna, and the improved 8 × 8 MIMO antenna is shown in Figure 10. The antenna pair is folded 90° along the long edge of the ground plane of the substrate, the radiating antenna element is perpendicular to the substrate, and all other parameters are the same as the planar antenna. By placing the antenna vertically, the ground clearance is reduced to zero. The performance of the vertically placed 8 × 8 MIMO antenna is consistent with that of the planar MIMO antenna, and the simulation and test results are not given for the sake of brevity.

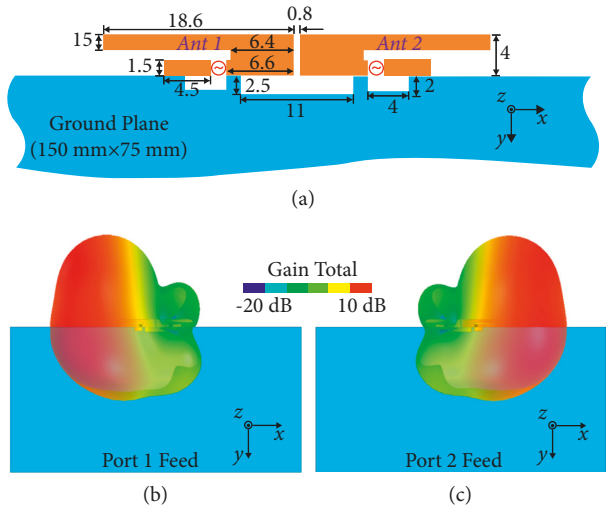

Figure 4: (a) Geometry and dimensions of the proposed MIMO antenna pair (Unit: mm). Simulated 3-D radiation patterns of the antenna pair when fed through (b) port1 and (c) port2.

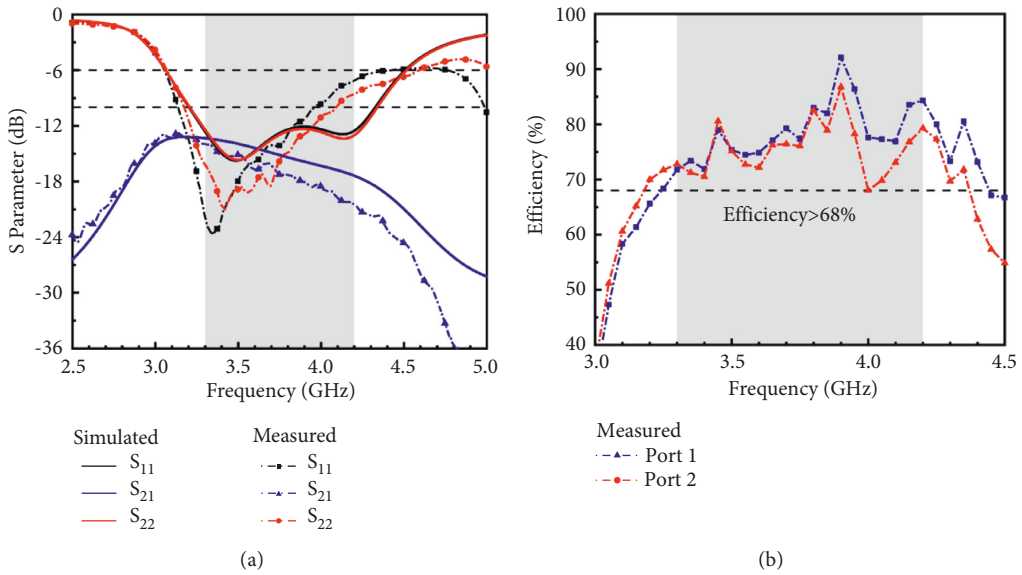

Figure 5: (a) Simulated and measured S parameter. (b) Measured efficiency of the antenna pair.

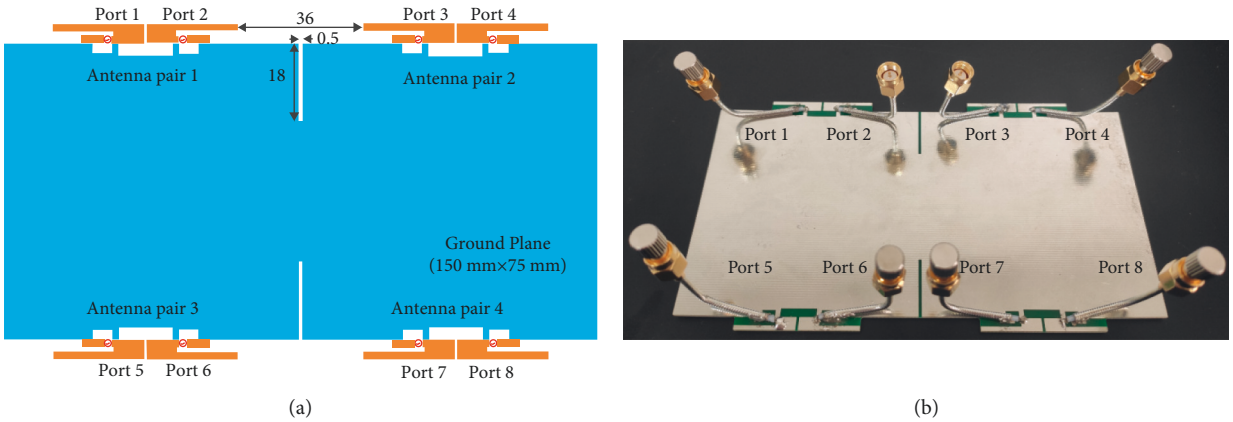

Figure 6: (a) Geometry and dimensions of the proposed 8 × 8 MIMO antenna. (b) Photograph of the proposed 8 × 8 MIMO antenna (unit: mm).

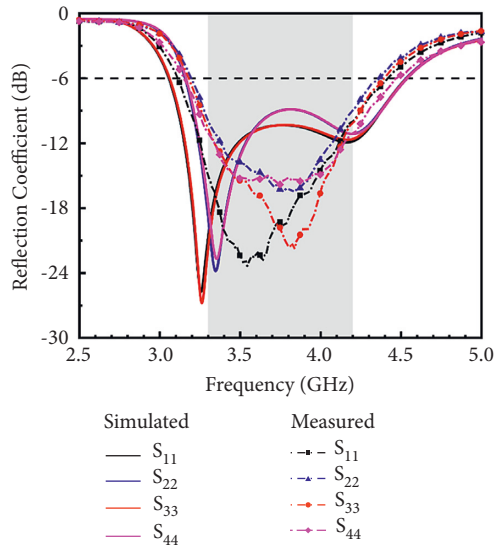

Figure 7: Simulated and measured reflection coefficients of the proposed 8 × 8 MIMO antenna.

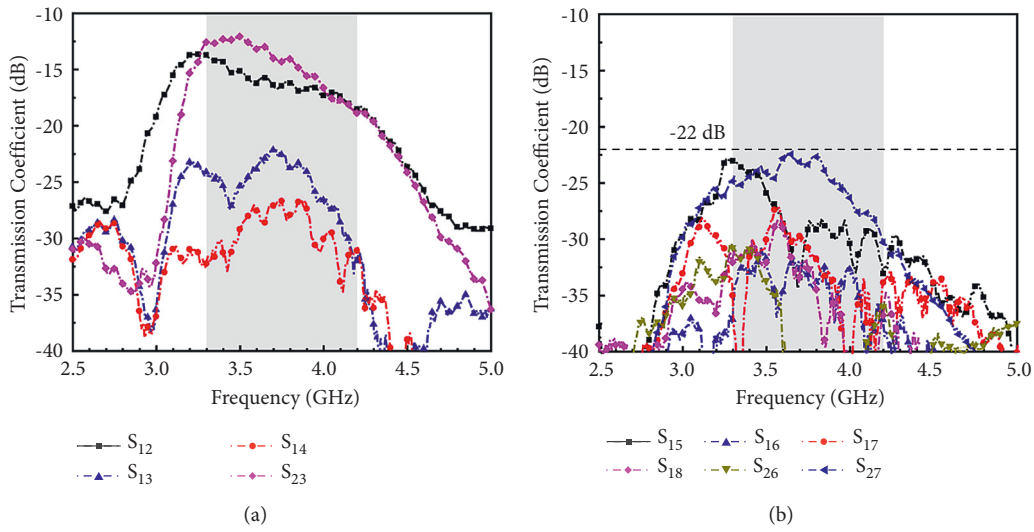

Figure 8: Measured isolation between (a) antenna pair 1 and antenna pair 2, (b) antenna pair 1, antenna pair 3, and antenna pair 4.

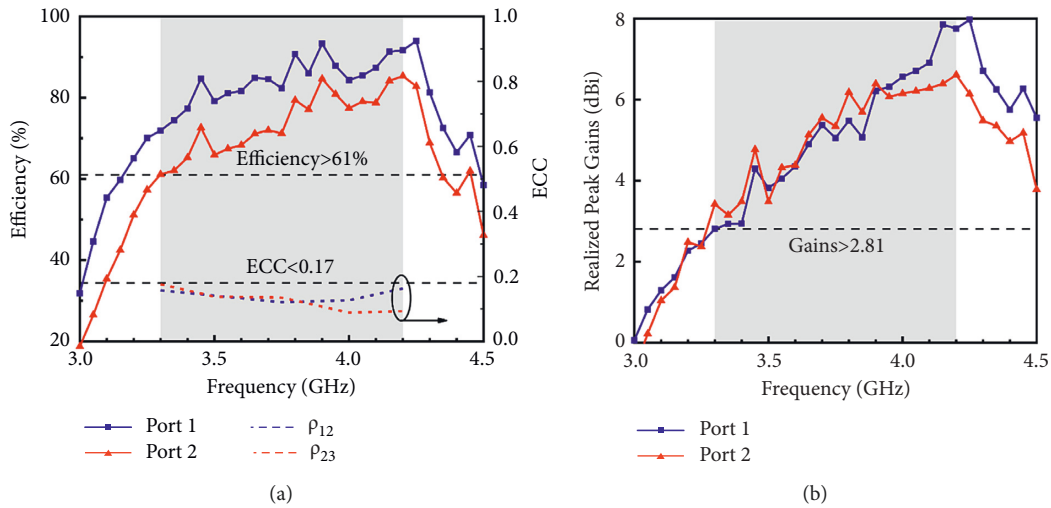

Figure 9: Measured efficiency, ECC, and gain of the proposed 8 × 8 MIMO antenna.

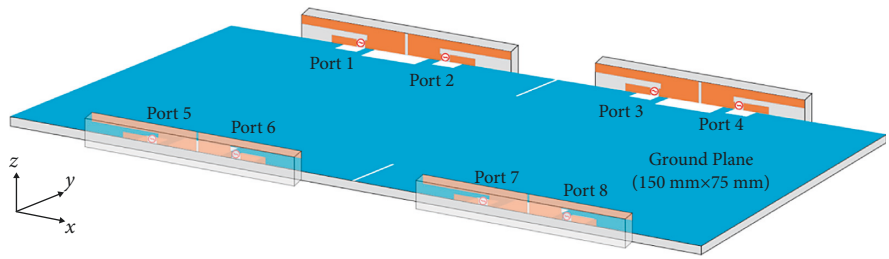

Figure 10: Vertically placed 8 × 8 MIMO antenna (unit: mm).

Table 1: Comparison of the proposed antennas with other works for 5G smartphones.

Ref.	Size (mm × mm)	Bandwidth (GHz)	Efficiency	ECC	Isolation (dB)	Numbers
[13]	20.6 × 9	3.35–3.67	56%–72%	<0.1	>17	8 × 8
[14]	28.4 × 6	3.40–3.68	59%–73%	<0.05	>16	8 × 8
[15]	32 × 7	3.34–3.65	64%–80%	<0.1	>15	8 × 8
[16]	20 × 6.2	3.36–3.70	58%–74%	<0.1	>17	4 × 4
[17]	20 × 6.2	3.28–4.00	52%–74%	<0.1	>12	2 × 2
[20]	25 × 7	3.36–3.64	35.2%–64.7%	<0.13	>12.7	4 × 4
[22]	25 × 10.5	3.33–3.67	40%–70%	<0.16	>14	8 × 8
[25]	36.6 × 6	3.25–6.15	47%–78%	<0.11	>15	8 × 8
[26]	30 × 7	3.25–7.50	40%–78%	<0.06	>10	4 × 4
[28]	40 × 7.5	3.30–5.05	31.6%–88.6%	<0.11	>12	8 × 8
[30]	30 × 7.5	3.31–4.20	63.1%–85.1%	<0.2	>10.5	8 × 8
Proposed	**38 × 4**	**3.18–4.40**	**61.14%–93.97%**	**<0.17**	**>12.25**	**8 × 8**

Table 1 compares the proposed wideband low-profile antenna with other existing antennas. First, the antenna element proposed in this paper has obvious advantages in the low-profile design. Other antenna profiles are above 6 mm, while the profile height of the antenna element in this paper is only 4 mm, which is much better than other antennas in Table 1. Second, the efficiency of the antenna proposed is 61.14–93.97%, which is the highest radiation efficiency in Table 1. It achieves high radiation efficiency while achieving a low-profile design, which also has significant advantages compared with other antennas. In addition, the antennas in [13–16, 20, 22] are all narrowband antennas operating at 3.4–3.6 GHz, while the bandwidth of the proposed wideband antenna is 3.18–4.40 GHz, which can fully cover n77 and n78 in 5G NR. While maintaining the wideband, low profile, and high radiation efficiency, the isolation of this antenna is acceptable, and the isolation proposed is better than [17, 26, 28, 30]. The ECC is also similar, because the two antenna elements of this antenna pair are arranged tightly, and the distance between the elements is only 0.8 mm, which has a certain influence on the correlation, but it has also far met the requirement that the ECC of mobile phone antenna is less than 0.5. In summary, compared with the existing work, this antenna has significant advantages of low profile, wide bandwidth, and high efficiency and will have an important application value in the future 5G ultrathin mobile phone.

4. Conclusion

A wideband 8 × 8 MIMO antenna for 5G ultrathin smartphones is designed in this paper. First, based on the traditional inverted-F antenna, a pair of base antenna pairs with a tight arrangement and low profile is designed. Then, the grounding surface edge structure is adjusted, and the contact area between the antenna element and grounding surface is changed, to optimize the impedance bandwidth and isolation of the antenna pair. A low-profile wideband 2-element antenna pair covering 5G new radio band n77 is designed with a profile height of only 4 mm. The results of simulation and measurement verify the excellent performance of the antenna pair. Based on this antenna pair, an 8-element MIMO antenna is further designed. The measured results show that its frequency band covers 3.18–4.40 GHz, the isolation between any two ports is less than −12.25 dB, the ECC is lower than 0.17, and the average port efficiency is 84.54%. In the current and future 5G ultrathin smartphones, the proposed antenna with low profile, high radiation efficiency, and simple structure has important application prospects. Of course, there are still some challenges in the design of low-profile wideband MIMO antennas. For example, the coverage frequency band is continued to expand on the basis of low profile to cover more bands such as n79/WLAN. At the same time, further improving the isolation of low-profile wideband MIMO antennas is also an important challenge.

Data Availability

The data that support the findings of this study are available from the corresponding author upon reasonable request.

Conflicts of Interest

The authors declare that they have no conflicts of interest.

Authors' Contributions

Hui Zhou and Di Wu contributed equally to this work.

Acknowledgments

This study was supported by the funds of the National Natural Science Foundation of China under grant nos. 11972333, 11902316, and 51902300 and the Natural Science Foundation of Zhejiang Province under grant nos. LZ19A020001, LY21F010011, and LQ19F010005. The authors would like to express their sincere appreciation for these supports.

References

[1] Z. Ren and A. Zhao, "Dual-band MIMO antenna with compact self-decoupled antenna pairs for 5G mobile applications," *IEEE Access*, vol. 7, pp. 82288–82296, 2019.

[2] M. Shafi, A. F. Molisch, P. J. Smith et al., "5G: a tutorial overview of standards, trials, challenges, deployment, and practice," *IEEE Journal on Selected Areas in Communications*, vol. 35, no. 6, pp. 1201–1221, 2017.

[3] H.-D. Chen, Y.-C. Tsai, C.-Y.-D. Sim, and C. Kuo, "Broadband eight-antenna array design for sub-6 GHz 5G NR bands metal-frame smartphone applications," *IEEE Antennas and Wireless Propagation Letters*, vol. 19, no. 7, pp. 1078–1082, 2020.

[4] C.-Y.-D. Sim, H.-Y. Liu, and C.-J. Huang, "Wideband MIMO antenna array design for future mobile devices operating in the 5G NR frequency bands n77/n78/n79 and LTE band 46," *IEEE Antennas and Wireless Propagation Letters*, vol. 19, no. 1, pp. 74–78, 2020.

[5] J. Huang, G. Dong, Q. Cai, Z. Chen, L. Li, and G. Liu, "Dual-band MIMO antenna for 5G/WLAN mobile terminals," *Micromachines*, vol. 12, no. 5, p. 489, 2021.

[6] K.-L. Wong, Y.-H. Chen, and W.-Y. Li, "Decoupled compact ultra-wideband MIMO antennas covering 3300-6000 MHz for the fifth-generation mobile and 5GHz-WLAN operations in the future smartphone," *Microwave and Optical Technology Letters*, vol. 60, pp. 2345–2604, 2018.

[7] C.-Z. Han, L. Xiao, Z. Chen, and T. Yuan, "Co-located self-neutralized handset antenna pairs with complementary radiation patterns for 5G MIMO applications," *IEEE Access*, vol. 8, pp. 73151–73163, 2020.

[8] Y. Li, C.-Y.-D. Sim, Y. Luo, and G. Yang, "High-isolation 3.5 GHz eight-antenna MIMO array using balanced open-slot antenna element for 5G smartphones," *IEEE Transactions on Antennas and Propagation*, vol. 67, no. 6, pp. 3820–3830, 2019.

[9] R. Li, Z. Mo, H. Sun, X. Sun, and G. Du, "A low-profile and high-isolated MIMO antenna for 5G mobile terminal," *Micromachines*, vol. 11, no. 4, p. 360, 2020.

[10] A. Zhao and Z. Ren, "Size reduction of self-isolated MIMO antenna system for 5G mobile phone applications," *IEEE Antennas and Wireless Propagation Letters*, vol. 18, no. 1, pp. 152–156, 2019.

[11] Y.-L. Ban, C. Li, C. Y. D. Sim, K.-L. Wong, and K. L. Wong, "4G/5G multiple antennas for future multi-mode smartphone applications," *IEEE Access*, vol. 4, pp. 2981–2988, 2016.

[12] L. Sun, H. Feng, Y. Li, and Z. Zhang, "Compact 5G MIMO mobile phone antennas with tightly arranged orthogonal-mode pairs," *IEEE Transactions on Antennas and Propagation*, vol. 66, no. 11, pp. 6364–6369, 2018.

[13] H. Piao, Y. Jin, and L. Qu, "A compact and straightforward self-decoupled MIMO antenna system for 5G applications," *IEEE Access*, vol. 8, pp. 129236–129245, 2020.

[14] A. Ren, Y. Liu, and C.-Y.-D. Sim, "A compact building block with two shared-aperture antennas for eight-antenna MIMO array in metal-rimmed smartphone," *IEEE Transactions on Antennas and Propagation*, vol. 67, no. 10, pp. 6430–6438, 2019.

[15] H. Piao, Y. Jin, Y. Xu, and L. Qu, "MIMO ground-radiation antennas using a novel closed-decoupling-loop for 5G applications," *IEEE Access*, vol. 8, pp. 142714–142724, 2020.

[16] Z. Ren, A. Zhao, and S. Wu, "MIMO antenna with compact decoupled antenna pairs for 5G mobile terminals," *IEEE Antennas and Wireless Propagation Letters*, vol. 18, no. 7, pp. 1367–1371, 2019.

[17] K. L. Wong, B. W. Lin, and S. E. Lin, "High-isolation conjoined loop multi-input multi-output antennas for the fifth-generation tablet device," *Microwave and Optical Technology Letters*, vol. 61, no. 1, pp. 111–119, 2018.

[18] J. Guo, L. Cui, C. Li, and B. Sun, "Side-edge frame printed eight-port dual-band Antenna array for 5G smartphone applications," *IEEE Transactions on Antennas and Propagation*, vol. 66, no. 12, pp. 7412–7417, 2018.

[19] C. Deng, D. Liu, and X. Lv, "Tightly arranged four-element MIMO antennas for 5G mobile terminals," *IEEE Transactions on Antennas and Propagation*, vol. 67, no. 10, pp. 6353–6361, 2019.

[20] L. Chang, Y. Yu, K. Wei, and H. Wang, "Polarization-orthogonal Co-frequency dual antenna pair suitable for 5G MIMO smartphone with metallic bezels," *IEEE Transactions on Antennas and Propagation*, vol. 67, no. 8, pp. 5212–5220, 2019.

[21] S. Shoaib, I. Shoaib, N. Shoaib, C. Xiaodong, and C. G. Parini, "Design and performance study of a dual-element multiband printed monopole antenna array for MIMO terminals," *IEEE Antennas and Wireless Propagation Letters*, vol. 13, pp. 329–332, 2014.

[22] Z. Xu and C. Deng, "High-Isolated MIMO antenna design based on pattern diversity for 5G mobile terminals," *IEEE Antennas and Wireless Propagation Letters*, vol. 19, no. 3, pp. 467–471, 2020.

[23] C. Y. Hsu, L. T. Hwang, F. S. Chang, S. M. Wang, and C. F. Liu, "Investigation of a single-plate π-shaped multiple-input–multiple-output antenna with enhanced port isolation for 5 GHz band applications," *IET Microwaves, Antennas & Propagation*, vol. 10, no. 5, pp. 553–560, 2016.

[24] A. Chen, J. Zhang, L. Zhao, and Y. Yin, "A dual-feed MIMO antenna pair with one shared radiator and two isolated ports for fifth generation mobile communication band," *International Journal of RF and Microwave Computer-Aided Engineering*, vol. 27, no. 9, pp. 21146–21152, 2017.

[25] Y. Hei, J. He, and w. Li, "Wideband decoupled 8-element MIMO antenna for 5G mobile terminal applications," *IEEE Antennas and Wireless Propagation Letters*, vol. 20, no. 8, pp. 1448–1452, 2021.

[26] X.-T. Yuan, Z. Chen, T. Gu, and T. Yuan, "A wideband PIFA-pair-based MIMO antenna for 5G smartphones," *IEEE Antennas and Wireless Propagation Letters*, vol. 20, no. 3, pp. 371–375, 2021.

[27] L. Cui, J. Guo, Y. Liu, and C.-Y.-D. Sim, "An 8-element dual-band MIMO antenna with decoupling stub for 5G smartphone applications," *IEEE Antennas and Wireless Propagation Letters*, vol. 18, no. 10, pp. 2095–2099, 2019.

[28] L. Sun, Y. Li, Z. Zhang, and Z. Feng, "Wideband 5G MIMO antenna with integrated orthogonal-mode dual-antenna pairs for metal-rimmed smartphones," *IEEE Transactions on Antennas and Propagation*, vol. 68, no. 4, pp. 2494–2503, 2020.

[29] L. Sun, Y. Li, and Z. Zhang, "Wideband integrated quad-element MIMO antennas based on complementary antenna pairs for 5G smartphones," *IEEE Transactions on Antennas and Propagation*, vol. 69, no. 8, pp. 4466–4474, 2021.

[30] L. Sun, Y. Li, Z. Zhang, and H. Wang, "Self-decoupled MIMO antenna pair with shared radiator for 5G smartphones," *IEEE Transactions on Antennas and Propagation*, vol. 68, no. 5, pp. 3423–3432, 2020.